Combustion and Flame 283 (2026) 114556

Contents lists available at ScienceDirect

Combustion and Flame

journal homepage: www.sciencedirect.com/journal/combustion-and-flame

Kinetic studies of the mutual oxidation of dimethyl carbonate and ethylene in a jet stirred reactor

Bowen Liu, Yuntian Guo, Rui Bo, Shuyan Guo, Hao Zhao *

School of Mechanics and Engineering Science, Peking University, Beijing 100871, China

ARTICLE INFO

Keywords:
Dimethyl carbonate (DMC)
Ethylene (C_2H_4)
Oxidation
Thermal runaway (TR)
Lithium-ion batteries (LiBs)

ABSTRACT

The mutual oxidation of dimethyl carbonate (DMC) and ethylene (C_2H_4) was investigated in a Jet Stirred Reactor (JSR) coupled with detailed kinetic modeling under fuel-lean ($\phi = 0.5$) and fuel-rich ($\phi = 2.0$) conditions over a temperature range of 800–1200 K. Experimental and numerical analyses revealed that C_2H_4 blending modulated the oxidation pathway of DMC by enlarging the radical pool through the early-stage oxidation of C_2H_4, which promoted DMC oxidation at lower temperatures. Specifically, the contribution of the oxidation pathway (DMC to DMC radicals) increases from 78.6% to 83.6% of the total DMC consumption with 20% C_2H_4 blending under the fuel-lean condition at 1050 K. Both Sun's model (Sun et al., Combust. Flame 164 (2016) 224–238) and Alzueta's model (Alzueta et al., Combust. Flame 188 (2018) 212–226) reasonably reproduce the evolution of the major species mole fraction with temperature, but overestimate the consumption of DMC above 1075 K and the production of minor intermediates, such as CH_4, C_2H_6, DME, and CO. The Alzueta's model has been updated to improve its predictive capability. In addition, for the DMC and C_2H_4 blends under fuel-rich conditions, the mole fraction of C_2H_4 slightly rises (from 1025 to 1125 K) followed by eventual depletion (above 1125 K), owing to the competition between radical-driven consumption of C_2H_4 and DMC oxidation-driven regeneration of C_2H_4. These findings provide kinetic evidence for understanding the mechanism of the interactions between C_2H_4 and DMC during thermal runaway in lithium-ion batteries (LiBs).

Novelty and significance statement

The novelty of this study lies in elucidating the kinetic interaction mechanisms between dimethyl carbonate (DMC) and ethylene (C_2H_4) related to the thermal runaway of lithium-ion batteries (LiBs). We reveal how C_2H_4 blending changes the DMC oxidation through the radical-driven pathways. This work provides important support for understanding LiB thermal runaway and fires, driven by such interactions, which pose catastrophic risks including combustible gas explosions, electrolyte depletion, and cascading cell failure. Our findings bridge combustion chemistry and battery safety engineering, offering a roadmap to design crosstalk-resistant electrolytes for next-generation energy storage systems.

1. Introduction

Lithium-ion batteries (LiBs) have revolutionized energy storage technologies, powering devices ranging from portable electronics to electric vehicles (EVs) and grid-scale renewable energy systems [1,2]. However, persistent safety concerns, such as thermal runaway (TR) [3–6], result in critical barriers to the development of advanced LiBs. TR can trigger catastrophic failures, including fires, explosions, and toxic gas emissions [7–9]. Crucially, the single-cell failure may further generate excess heat to trigger fires in adjacent cells. Several recent high-profile electric vehicle accidents [3,10,11] caused by TR propagation have intensified public and regulatory concerns regarding the safety of EVs.

TR in LiBs is typically initiated by mechanical damage [13], thermal abuse [6], and further by internal short circuits [12], leading to sequential degradations of electrolyte solvents (e.g., dimethyl carbonate [DMC], diethyl carbonate [DEC], and ethyl methyl carbonate [EMC]), separators, and electrode materials [10]. Among these degradation processes, electrolyte decomposition and oxidation dominate heat

* Corresponding author.
E-mail address: h.zhao@pku.edu.cn (H. Zhao).

https://doi.org/10.1016/j.combustflame.2025.114556
Received 18 July 2025; Received in revised form 15 October 2025; Accepted 16 October 2025
Available online 23 October 2025

Table 1
A review of experiments related to the combustion characteristics of DMC. (LBV: laminar burning velocity; IDT: ignition delay time; SP: speciation; T_0: initial temperature; T_5, P_5: reflected-shock temperature and pressure; T_C, P_C: compression temperature and pressure; T_f: flame temperature;).

Mixture	Equivalent ratio, ϕ	Temperature range (K)	Pressure (atm)	Experiments	Refs.
DMC/O_2/N_2	2.5; 5.0; ∞	850–1100	1.0	Jet stirred reactor; SP;	[17]
DMC/N_2	∞	1075–1475	1.0	Flow reactor; SP;	[19]
DMC/O_2/N_2	1.0; ∞	700–1200	1.0	Micro flow reactor; SP;	[25]
DMC/Ar	∞	842–1490	0.04; 0.2; 1.0	Flow reactor; SP;	[21]
DMC/O_2/N_2	0.03–1.56	500–1073	20; 40; 60	Flow reactor; SP;	[26]
DMC/air	0.84–1.32	T_0=300	1.0	Spherically propagating flame; LBV;	[28]
DMC/air	0.7–1.5	T_0=318–423	1.0	Spherically propagating flame; LBV;	[29]
DMC/air	0.7–1.5	T_0=373	1–8	Spherically propagating flame; LBV;	[30]
DMC/air	0.65–1.6	T_0=298–358	1.0	Heat flux; LBV;	[31]
DMC/O_2/Ar	0.5–2.0	T_5=1100–1600	P_5 = 1.2, 5.0, 10	Shock tube; IDT;	[32]
DMC/O_2/Ar	0.5–2.0	T_C/T_5=795–1585	P_C/P_5 = 2.0, 20, 40	Shock tube; Rapid compression machine; IDT;	[33]
DMC/O_2/Ar (He)	0.5–2.0	T_5=1307–1642	P_5 = 1.25–1.33	Shock tube; IDT;	[29]
DMC/O_2/Ar	0.5–2.0	T_C/T_5=778–1102	P_C= 20–40	Rapid compression machine; IDT;	[34]

release and battery fire [14]. During TR, organic carbonates go through the pyrolysis pathway to form flammable intermediate gases, such as CO, CH_4, C_2H_4, H_2 [4,15], and the oxidation pathway with significant heat releases. In particular, the interaction and mutual oxidation of organic carbonates and flammable intermediates control the ignition and propagation of battery fire [16] and even explosion [7]. Despite extensive studies on flammable gas generation and oxidation during the LiB failure [4,7,14,16,17], the mutual oxidation kinetics between electrolyte solvents and pyrolyzed flammable gases within a battery remain poorly investigated in terms of coupling reactions, oxidation characteristics, and kinetic pathways.

Furthermore, multidirectional gas crosstalk between electrodes and electrolyte has been a key factor in exacerbating battery fires in LiBs. For example, ethylene (C_2H_4), a primary flammable intermediate in electrolytes closed to anode, can migrate to cathode, destabilize metal oxides, and then trigger O_2 release. The released O_2 diffuses back to electrolyte and anode, which accelerates the electrolyte degrading and further C_2H_4 production. As such, it creates a self-amplifying loop that escalates TR [18]. Simultaneously, C_2H_4 participates in the electrolyte oxidation in a competitive or synergic manner. Numerous studies have investigated the pyrolysis and oxidation of individual electrolyte solvent, including DMC [17,19–22] and DEC [23–25]. Alexandrino et al. [26] performed the oxidation of DMC at high pressure (20, 40, and 60 bar) in a flow reactor. Sun et al. [21] investigated the pyrolysis of DMC under different pressure (40, 200, and 1040 mbar) using a flow reactor, and developed a detailed kinetic model for DMC pyrolysis consisting of 257 species and 1563 reactions. Kanayama et al. [25] compared the gas-phase reactivities of DMC, EMC, and DEC using a micro-flow reactor with a controlled temperature profile. The gas-phase reactivities of the three carbonate esters were found to follow the order DEC>DMC≈EMC. Nakamura et al. [23] measured species concentrations during the oxidation of DEC in a jet stirred reactor at 10 bar over a temperature range of 500–1200 K at equivalence ratios of 0.5, 1.0 and 2.0. They developed a chemical kinetic model for DEC including both high-temperature and low-temperature oxidation mechanisms, and compared the model predictions with the experimental data. Shahla et al. [27] investigated the DEC oxidation using a jet stirred reactor at atmospheric pressure. It was demonstrated that the molecular decomposition of the fuel is the main DEC consumption pathway. Zhao et al. [24] conducted oxidation experiments of DEC with ozone addition using a laminar flow reactor. The ozone (O_3) lowers the DEC oxidation onset to 450 K by supplying reactive oxygen atoms. Table 1 shows experimental

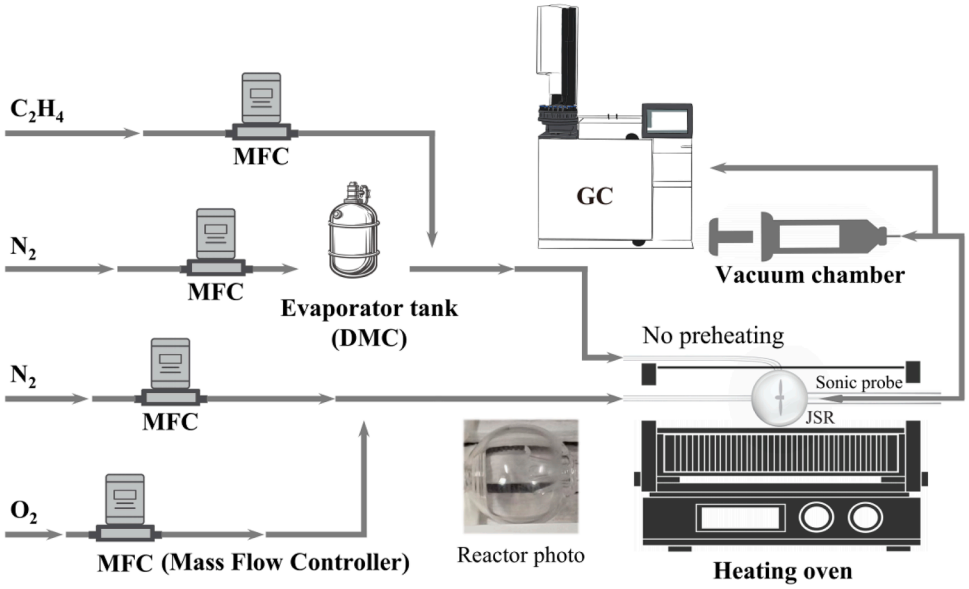

Fig. 1. Experimental setup.

Table 2
Experimental conditions.

Case	Residence time (s)	Equivalent ratio, ϕ	Percentage of components (%)				Temperature range (K)	Flow rate (ml/min)
			DMC	C_2H_4	O_2	N_2		
1	0.27 - 0.18	0.5	0.30	0.00	1.80	97.90	800 - 1200	2500
2		2.0	0.30	0.00	0.45	99.25		
3		0.5	0.27	0.03	1.80	97.90		
4		2.0	0.27	0.03	0.45	99.25		
5		0.5	0.24	0.06	1.80	97.90		
6		2.0	0.24	0.06	0.45	99.25		

studies on the combustion properties of DMC. While previous research has advanced the kinetic understanding of electrolyte solvents, real battery fire scenarios involve complex mixtures of multiple flammable gases and exhibit pronounced crosstalk. The chemical kinetic interactions between flammable intermediate gases and electrolyte solvents remain unclear for understanding LiB fires.

Therefore, this work investigates the mutual oxidation of flammable intermediate such as C_2H_4 and electrolyte solvents such as DMC from 800 K to 1200 K in an atmospheric pressure Jet Stirred Reactor (JSR) for understanding its impact on LiB fires. Species concentrations, including DMC, C_2H_4, CH_4, CH_3OCH_3 (DME), C_2H_6, C_2H_2, O_2, CO, and CO_2, are quantified by using gas chromatography. Experimental results are compared with model predictions using two recently developed DMC mechanisms. Key reactions and oxidation pathways are identified through the reaction path analysis, sensitivity analysis, and radical pool quantification.

2. Methods

2.1. Experimental methods

The oxidation experiments were conducted in a JSR system at atmospheric pressure, as shown in Fig. 1. The core reactor, made of fused quartz with an internal volume of 30.5 cm^3, was specifically designed to

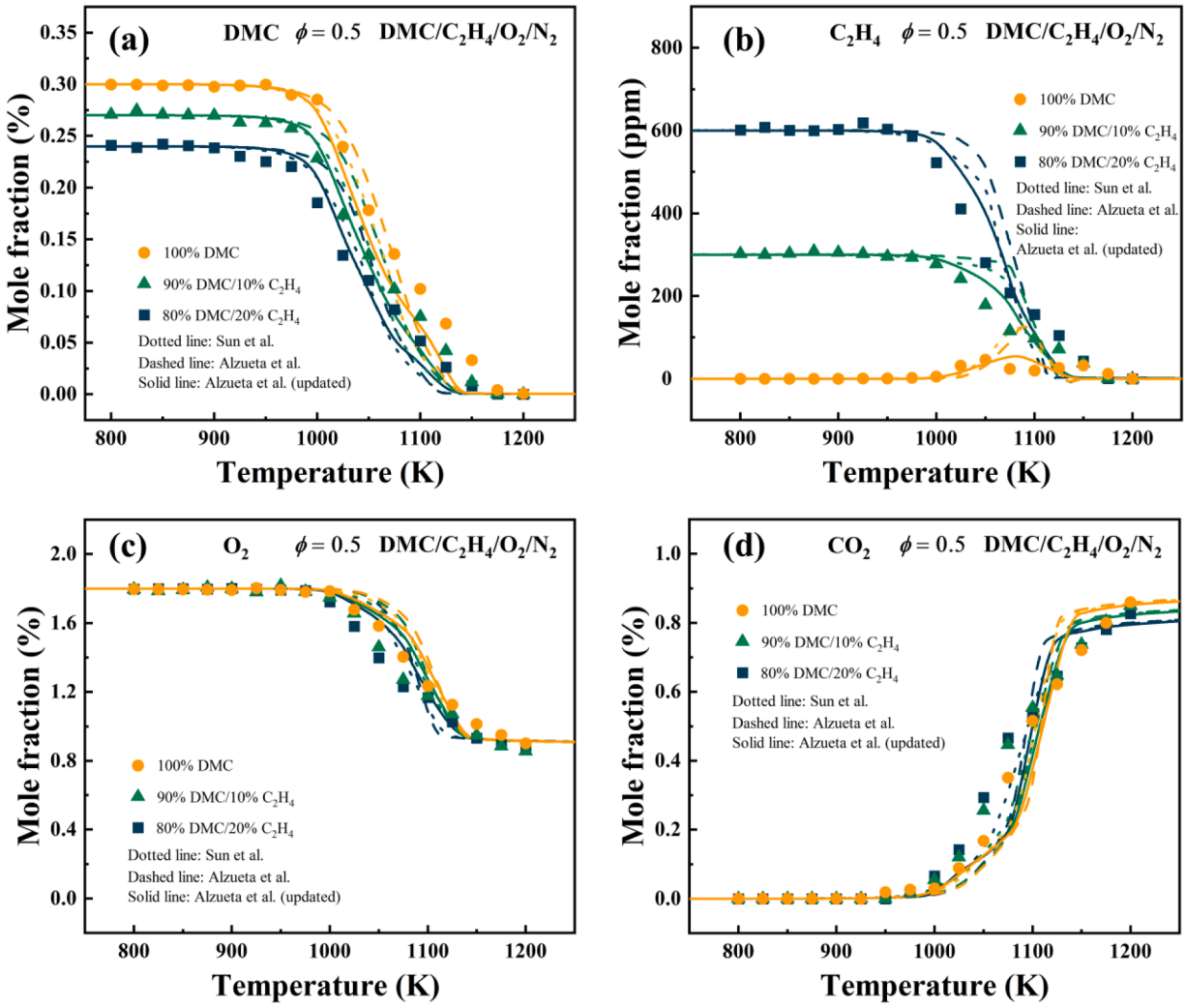

Fig. 2. Mole fractions of major species as a function of temperature at $\phi = 0.5$ with different C_2H_4 blending ratios. The symbols represent the experimental data and the curves represent predictions of models, where the dotted, dashed, and solid lines represent the predictions of Sun's model, Alzueta's model and updated Alzueta's model, respectively. (a) DMC; (b) C_2H_4; (c) O_2; (d) CO_2.

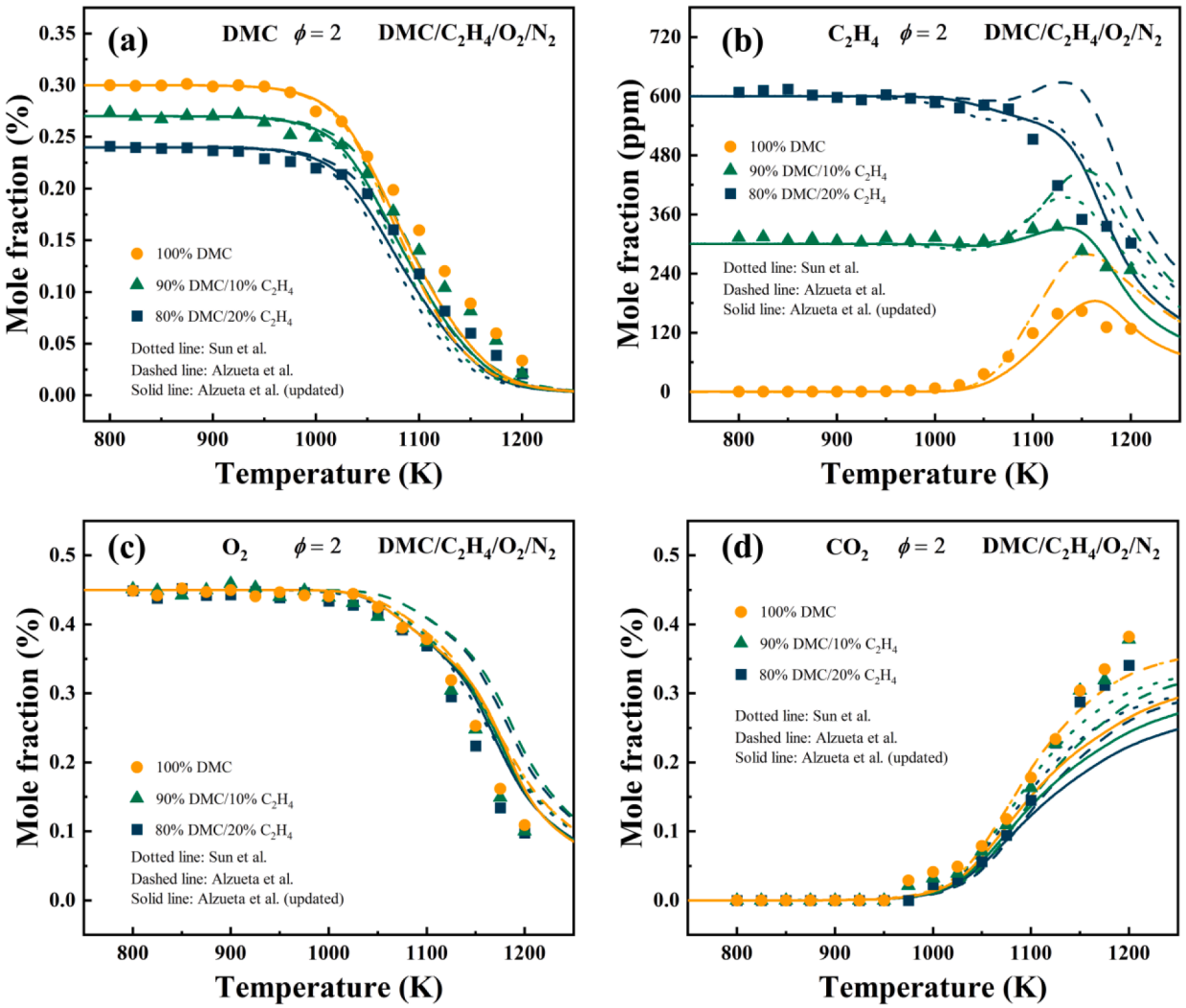

Fig. 3. Mole fractions of major species as a function of temperature at $\phi = 2.0$ with different C_2H_4 blending ratios. The symbols represent the experimental data and the curves represent predictions of models, where the dotted, dashed, and solid lines represent the predictions of Sun's model, Alzueta's model and updated Alzueta's model, respectively. (a) DMC; (b) C_2H_4; (c) O_2; (d) CO_2.

minimize wall reactions. Similar to the design by Dagaut et al. in [35], the reactor incorporates four centrally positioned nozzles of 1 mm inner diameter to generate intense turbulence and ensure homogeneous mixing. The reactant delivery system consisted of four streams, including the oxidizer stream, liquid fuel supply (DMC), ethylene blending stream, and the primary nitrogen stream. Liquid DMC was introduced into a preheated vaporization chamber via a high-precision syringe pump (CHEMYX FUSION 6000-X), subsequently carried by secondary nitrogen flow. The vaporized DMC stream merged with the ethylene before entering the reactor. The blending fuel stream was introduced to the inlet of JSR through a 2 mm inner diameter quartz fuel tube (5.5 cm length, 0.17 cm^3 vol) that passed through a hole in the side wall of the heating oven. Subsequently, the blending fuel stream and mainstream nitrogen/oxygen were merged at the JSR inlet. Notably, the fuel tube occupied only 0.57 % of the JSR total volume to prevent over-preheating. Post-reaction gases were sampled through a 100 μm inner diameter sonic probe at the reactor outlet, coupled to a vacuum chamber to minimize flow disturbance of JSR and limit residence time in the transfer line. Temperatures at three locations inside the JSR (inlet, center, and outlet) were calibrated from 800 to 1200 K using a K-type thermocouple with an uncertainty of ±2.5 K. Gaseous reactants were precisely controlled using mass flow controllers (MKS Instruments, ±0.5 % uncertainty), which were calibrated using a gas calibrator (Drycal 530+, ±1 % accuracy). The purity of the gases was greater than 99.999 %. Product analysis was conducted using a gas chromatograph (Agilent 8890) equipped with dual flame ionization detectors (FID) and a thermal conductivity detector (TCD). Species quantification involved more than two complete measurement repetitions under each experimental condition, demonstrating a relative deviation of <5 % in repeatability tests.

2.2. Experimental conditions

The experimental conditions in this study are listed in Table 2. The inlet volumetric flow rate is fixed at 2500 ml/min at 298 K, while the residence time (τ) can be calculated by:

$$\tau = \frac{V_0}{u} \cdot \frac{T_0}{T} \quad (1)$$

where V_0, u, T_0, and T represent the internal volume of JSR, the total volumetric flow rate of the JSR inlet at room temperature, room temperature at 298 K, and the temperature in JSR, respectively.

2.3. Numerical simulations

Numerical simulations were conducted using Chemkin-Pro [36] to

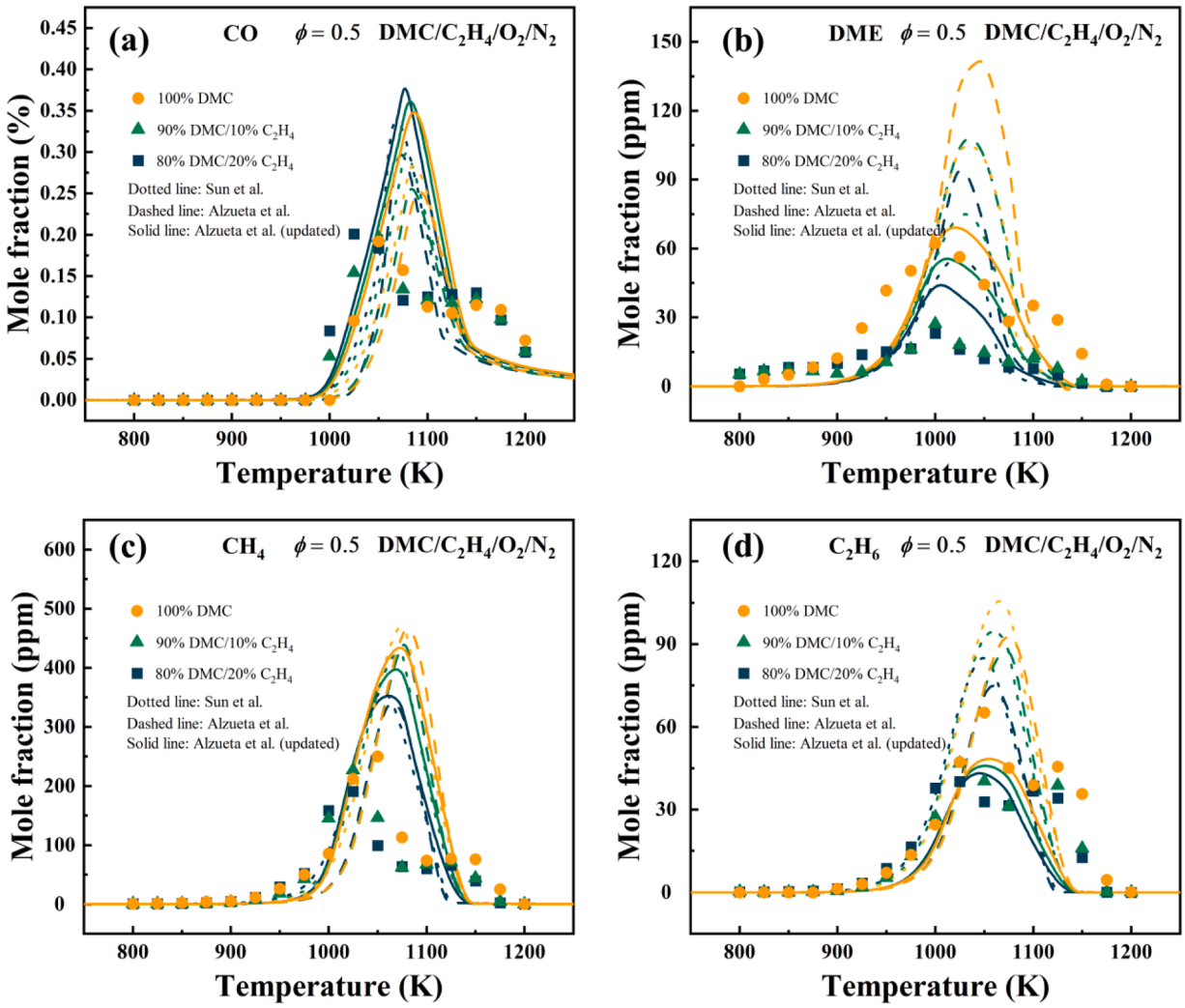

Fig. 4. Mole fractions of minor species as a function of temperature at $\phi = 0.5$ with different C_2H_4 blending ratios. The symbols represent the experimental data and the curves represent predictions of models, where the dotted, dashed, and solid lines represent the predictions of Sun's model, Alzueta's model and updated Alzueta's model, respectively. (a) CO; (b) DME; (c) CH_4; (d) C_2H_6.

analyze DMC oxidation kinetics. Two detailed chemical kinetic mechanisms, the model of Sun et al. [21] and the model of Alzueta et al. [33], were employed to interpret experimental results and evaluate the kinetic behavior. The model of Sun et al. was developed by combining the AramcoMech 1.3 base framework [37] with a 23-reaction DMC simplified sub-mechanism. In comparison, the model of Alzueta et al. adopted the original DMC sub-mechanism of Glaude et al. [38], and optimized the thermodynamic data for the species involved in the DMC oxidation. Based on the Alzueta et al. model, the rate coefficients for four key reactions were updated to enhance the model predictive performance. The complete updated mechanism can be found in the Supplementary Material.

3. Results and discussion

3.1. The mole fraction of species

The temperature-dependent mole fractions of major species under fuel-lean conditions at $\phi = 0.5$ with varying C_2H_4 blending ratios are depicted in Fig. 2, including DMC, C_2H_4, O_2, and CO_2. As shown in Fig. 2 (a), the blending of C_2H_4 (up to 20 %) marginally affects the oxidation of DMC, with the onset oxidation temperature of DMC dropping by approximately 25 K. Moreover, with 10 % and 20 % C_2H_4 blending, despite the presence of C_2H_4 production pathways from DMC decomposition, the mole fraction of C_2H_4 is observed to decrease monotonically with increasing temperature under the fuel-lean condition, as is depicted in Fig. 2(b). This strongly suggests that C_2H_4 consumption through oxidation pathways (e.g., reactions with OH/O radicals) dominates over its production from DMC decomposition under fuel-lean conditions. The experimental trends in the mole fractions of major species are successfully reproduced by the updated Alzueta's model. Notably, all models underestimate the DMC mole fraction above 1075 K across all C_2H_4 blending levels in Fig. 2(a).

The evolutions of major species mole fraction under fuel-rich conditions at $\phi = 2.0$ with varying C_2H_4 blending ratios are depicted in Fig. 3, including DMC, C_2H_4, O_2, and CO_2. Fig. 3(a) shows the DMC mole fraction decreases monotonically with the temperature, consistent with the high-temperature chemical kinetic behavior of oxygenated hydrocarbons [23]. Significantly, the mole fraction of C_2H_4 exhibits a characteristic non-monotonic profile as a function of temperature at a 10 % C_2H_4 blending ratio in Fig. 3(b). The mole fraction of C_2H_4 slightly rises (from 1025 to 1125 K) followed by eventual depletion (above 1125 K). This multiphase behavior is mainly attributed to competition between C_2H_4 consumption through reactions with radicals and its regeneration through the pyrolysis and oxidation of DMC. In addition, the intermediate regeneration peak for the mole fraction of C_2H_4 is relatively lower when the percentage of C_2H_4 reaches 20 %. Furthermore, the observed non-monotonic behavior of C_2H_4 mole fraction highlights the complex

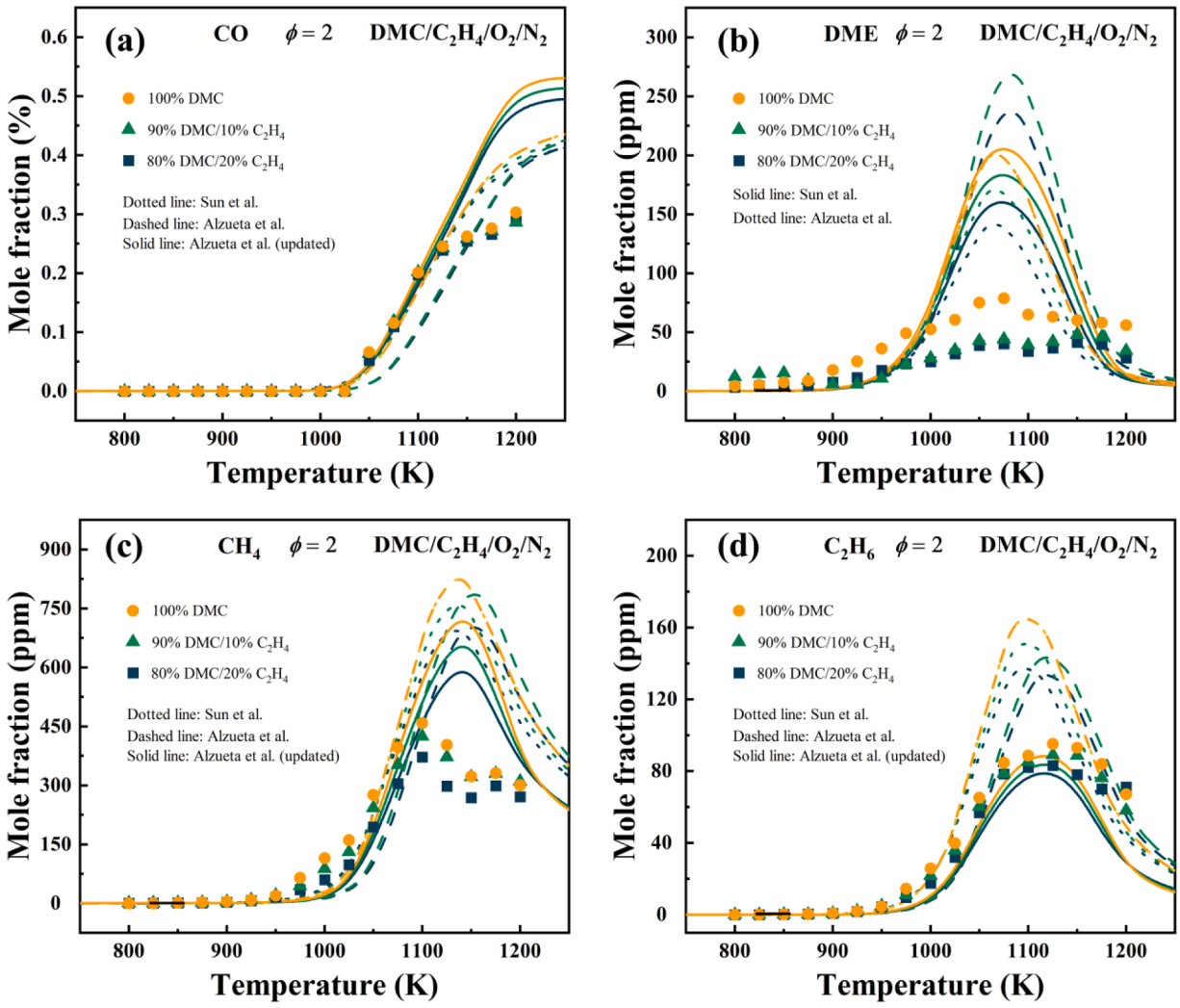

Fig. 5. Mole fractions of minor species as a function of temperature at $\phi = 2.0$ with different C_2H_4 blending ratios. The symbols represent the experimental data and the curves represent predictions of models, where the dotted, dashed, and solid lines represent the predictions of Sun's model, Alzueta's model and updated Alzueta's model, respectively. (a) CO; (b) DME; (c) CH_4; (d) C_2H_6.

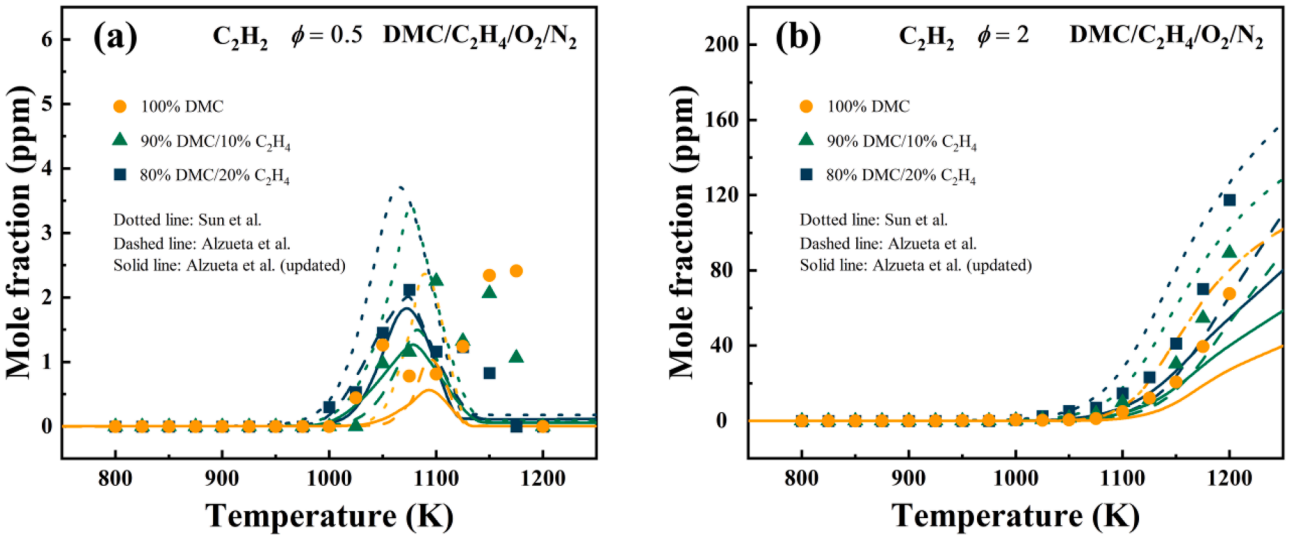

Fig. 6. Mole fractions of C_2H_2 as a function of temperature at $\phi = 0.5$ and $\phi = 2.0$ with different C_2H_4 blending ratios. The symbols represent the experimental data and the curves represent predictions of models, where the dotted, dashed, and solid lines represent the predictions of Sun's model, Alzueta's model and updated Alzueta's model, respectively. (a) $\phi = 0.5$; (b) $\phi = 2.0$.

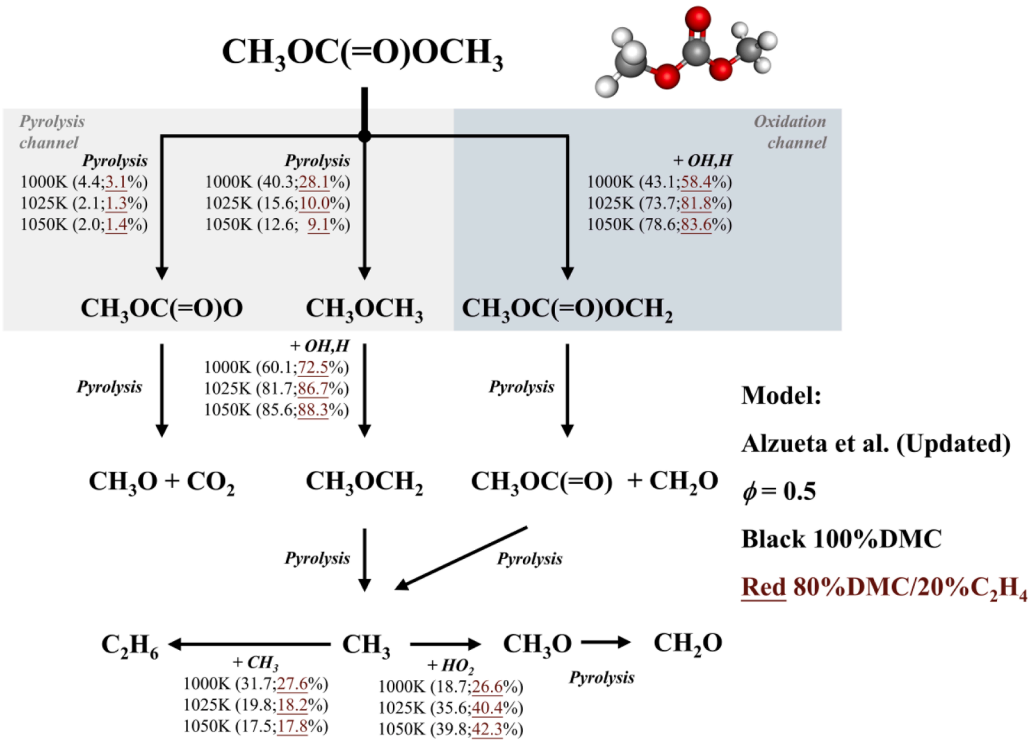

Fig. 7. The main consumption pathways of DMC at different temperatures under fuel-lean condition using the updated Alzueta's model. The black and red fonts represent the channel percentages for pure DMC and 20 % C_2H_4 blending, respectively.

interplay between its consumption and regeneration processes under fuel-rich conditions.

The mole fraction of minor species under fuel-lean ($\phi = 0.5$) and fuel-rich ($\phi = 2.0$) conditions are depicted in Fig. 4, Fig. 5, and Fig. 6, including CO, DME, CH_4, C_2H_6, and C_2H_2. Both the Alzueta's and Sun's models consistently overpredict minor species mole fractions in both fuel-lean and fuel-rich conditions. For instance, the mole fraction of DME is overestimated by nearly a factor of two in the temperature range from 1000 K to 1100 K, as is depicted in Fig. 4(b). The minor species mole fractions under fuel-rich conditions are significantly higher than those under fuel-lean conditions, and no significant C_2H_2 formation (less than 5 ppm) is observed under fuel-lean condition as is depicted in Fig. 6 (a). In contrast, fuel-rich conditions exhibit substantial C_2H_2 yields above 1100 K in Fig. 6(b).

3.2. Reaction pathway analysis

To elucidate the effect of C_2H_4 blending on the oxidation kinetics of DMC, the main consumption pathways of DMC under fuel-lean conditions at $\phi = 0.5$ are depicted in Fig. 7 using updated Alzueta's model. Three primary pathways are identified with two pyrolysis channels and one oxidation channel. As shown in Fig. 7, the contribution of oxidation channel to the DMC consumption increases from 78.6 % to 83.6 % with a 20 % C_2H_4 blending at 1050 K, while pyrolysis channels decrease. This shift is attributed to enhanced radical pools, such as O and OH radicals, generated through the oxidation of C_2H_4, which accelerate the H-abstraction reaction of DMC to produce the DMC radical, $CH_3OC(=O)OCH_2$. Then, the DMC radical undergoes two rapid pyrolysis steps to produce CH_2O, CO_2, and CH_3. Moreover, the DMC is converted to the CH_3OCH_3 (DME) through a pyrolysis channel, followed by oxidation of DME to its radicals, and other products. Additionally, the percentage of pyrolysis channels decreases relatively as the temperature increases from 1000 K to 1050 K.

The main pathways governing C_2H_4 evolution under fuel-rich conditions at $\phi = 2.0$ are analyzed in Fig. 8(a) using updated Alzueta's model. C_2H_4 is primarily generated through the oxidation of DMC, and consumed through reactions with O, OH, H, and CH_3 radicals. To explain the nonmonotonicity of C_2H_4 observed in Fig. 3(b), the oxidation of pure DMC and pure C_2H_4 under fuel-rich conditions is contrasted in Fig. 8(b). The onset temperature for the oxidation of C_2H_4 is about 875 K, which is about 100 K lower than the DMC oxidation (approximately 975 K). With increasing temperature, the oxidation of DMC produces C_2H_4, which triggers a competition between the DMC-derived C_2H_4 production and the radical-driven C_2H_4 consumption. In addition, the higher oxidation rate of DMC (steep slope in Fig. 8(b)) allows the production of C_2H_4 to dominate during the temperature range from 1025 K to 1125 K, leading to an increase in the mole fraction of C_2H_4. Above 1125 K, the consumption of C_2H_4 becomes dominant again due to the exhaustion of DMC and the enhanced oxidation of C_2H_4.

The interactions between C_2H_4 and electrolyte solvents, such as DMC, critically influences the thermal runaway in LiBs. Our findings reveal that C_2H_4 exhibits superior reactivity over DMC, promoting the radical pool enhancement. In turn, the DMC degradation is accelerated through radical-driven oxidation pathways, thereby amplifying the electrolyte depletion and heat release. Such synergistic interactions directly exacerbate the gas evolution, such as CO_2, CH_4, and C_2H_2, and pressure buildup.

3.3. Analysis of reaction sensitivity

The reaction sensitivity analyses of the DMC consumption with varying C_2H_4 blending are conducted by using updated Alzueta's model under fuel-lean and fuel-rich conditions in Fig. 9(a) and Fig. 9(b), respectively. The sensitivity coefficient S_i for DMC is defined as:

$$S_i = \frac{(\Delta X_{\mathrm{DMC}}/X_{\mathrm{DMC}})}{\Delta k_i/k_i} \tag{2}$$

where X_{DMC} is the mole concentration of DMC and k_i is the rate constant of i th reaction.

The sensitivity of the DMC consumption to key reactions under fuel-

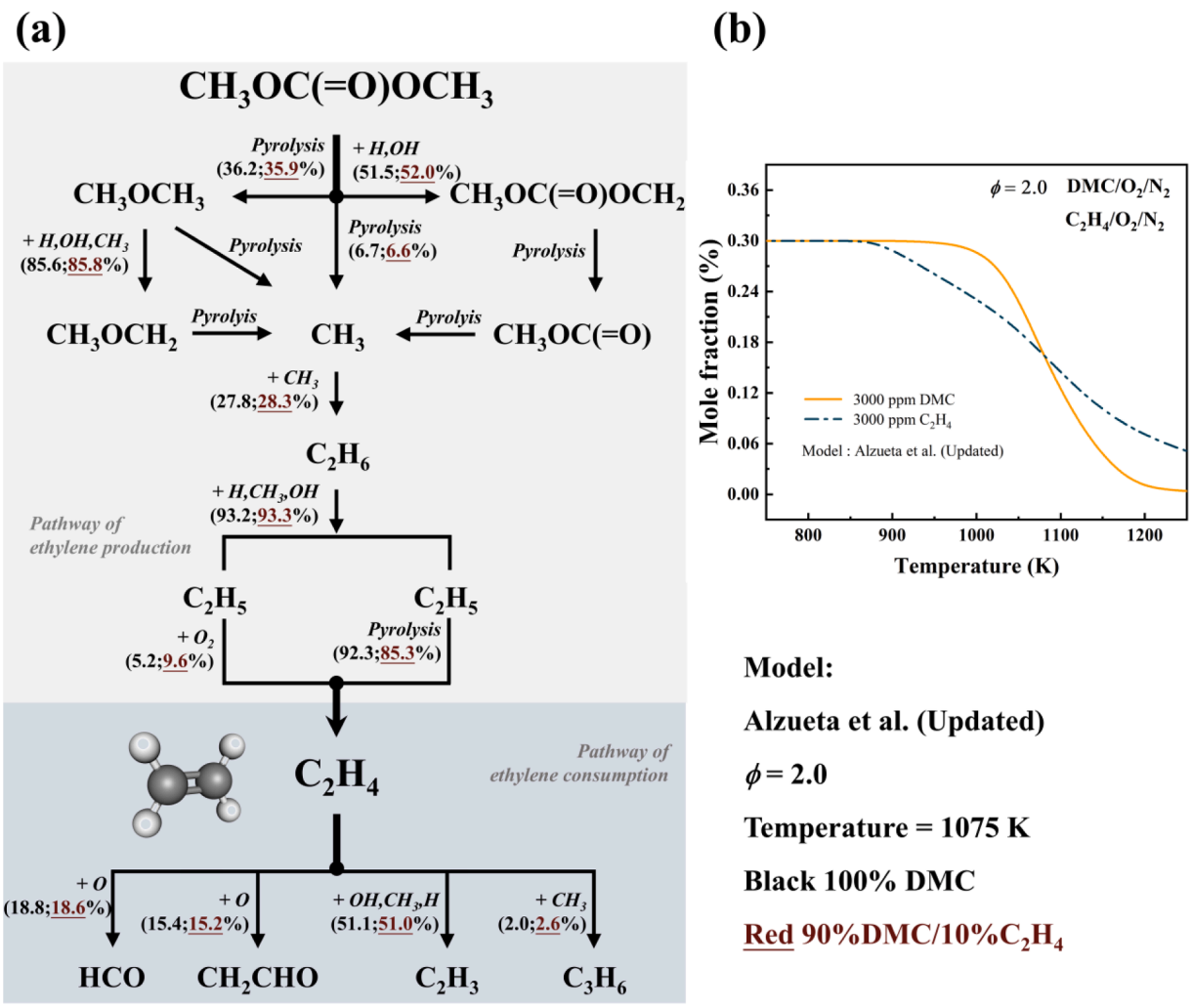

Fig. 8. (a) The main consumption and production pathways of C_2H_4 at 1075 K under fuel-rich condition using the updated Alzueta's model. The black and red fonts represent the channel percentages for pure DMC and 10 % C_2H_4 blending, respectively; (b) Mole fractions of DMC and C_2H_4 as a function of temperature at $\phi = 2.0$ under the oxidation of pure DMC and pure C_2H_4.

lean condition at $\phi = 0.5$ is quantified in Fig. 9(a). Reactions with negative sensitivity coefficients promote the DMC consumption. R10, $CH_3+HO_2 = CH_3O+OH$, exhibits the largest negative sensitivity coefficient, and the C_2H_4 blending enhances the sensitivity, as ethylene-derived radicals accelerate the formation of CH_3 and HO_2. Conversely, R1, $CH_3+HO_2 = CH_4+O_2$ shows the largest positive sensitivity, inhibiting the DMC consumption by scavenging CH_3 and HO_2 radicals to form the more stable products. Under fuel-rich conditions as shown in Fig. 9 (b), the reactions related to the DMC consumption shift to pyrolysis-related pathways due to restricted oxygen. The pyrolysis reactions, R12 and R13, have greater negative sensitivities, reflecting their dominant roles in the DMC decomposition under fuel-rich conditions. Moreover, the change in the sensitivity coefficient induced by C_2H_4 blending is minimal, which is consistent with the minor change in the percentage of reaction channels in Fig. 8(a)

3.4. Analysis of radical pool

To further analyze the effect of C_2H_4 blending on the oxidation of DMC, the radical pool analysis during the oxidation of DMC with different C_2H_4 blending ratios under fuel-lean and fuel-rich conditions are depicted in Fig. 10(a) and Fig. 10(b), respectively. The mole fractions of H and OH radicals increase across both fuel-lean and fuel-rich conditions. Under fuel-lean condition at $\phi = 0.5$, the mole fractions of H and OH radicals rise nearly doubled with 20 % C_2H_4 blending, in agreement with the enhanced oxidation pathways (e.g. the enhancement of H-abstraction reactions, $CH_3OC(=O)OCH_3+OH = CH_3OC(=O)OCH_2+H_2O$ and $CH_3OC(=O)OCH_3+H = CH_3OC(=O)OCH_2+H_2$) observed in Fig. 7. Similarly, H radicals exhibit an obvious increase, promoting chain-branching reactions, $H + O_2 = OH+O$, which accelerate the oxidation of DMC. Moreover, the radical amplification effect is markedly stronger under fuel-lean conditions due to abundant O_2, which facilitates the oxidation of C_2H_4 through the oxidation pathways, such as $C_2H_4+OH = C_2H_3+H_2O$. In summary, C_2H_4 can act as a radical promoter in the oxidation of DMC, and the radical-mediated synergy explains the accelerated DMC oxidation in Figs. 7 and 8. Under fuel-rich conditions, however, radical-driven oxidation of C_2H_4 competes with the pyrolysis and oxidation of DMC, leading to the nonmonotonic behavior of C_2H_4 mole fractions in Fig. 3(b).

4. Conclusions

The kinetic interactions between DMC and C_2H_4 under fuel-lean and fuel-rich conditions were systematically investigated using an atmospheric pressure Jet Stirred Reactor (JSR) coupled with detailed kinetic modeling. The main findings are summarized as follows.

C_2H_4 blending significantly enhances the oxidation pathways of DMC by increasing radical pools, such as O, OH, and CH_3, through the

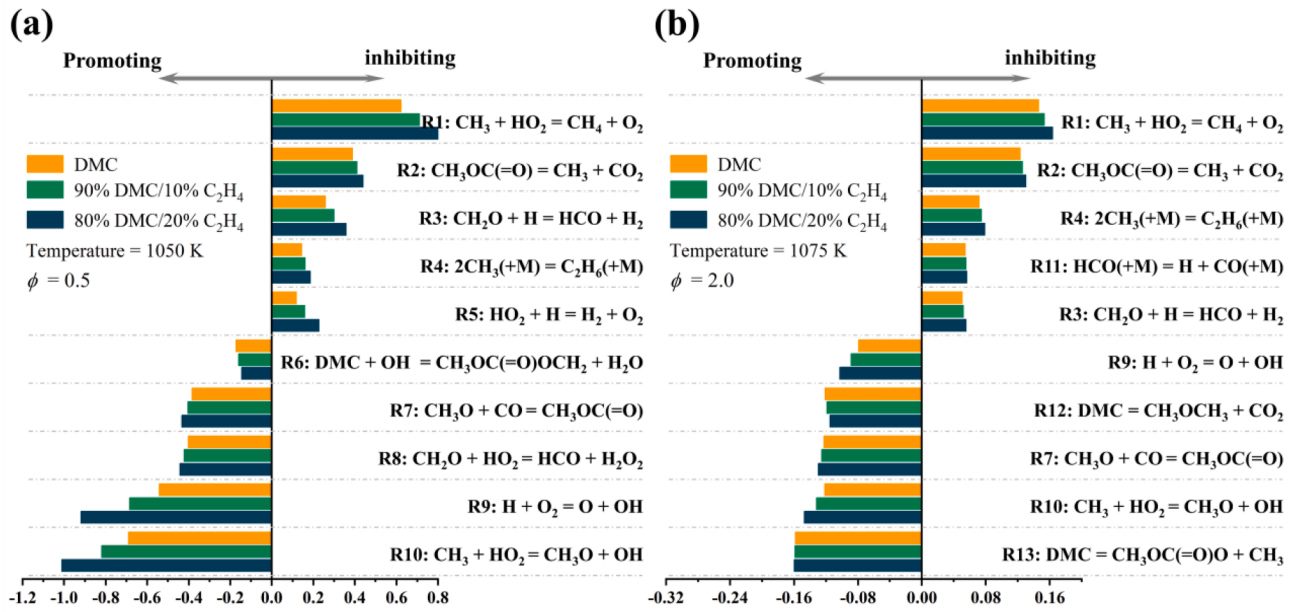

Fig. 9. Reaction sensitivity analysis of the DMC consumption using updated Alzueta's model. (a) 1050 K, $\phi = 0.5$, with 0 %, 10 %, and 20 % C_2H_4 blending;(b) 1075 K, $\phi = 2.0$, with 0 %, 10 %, and 20 % C_2H_4 blending.

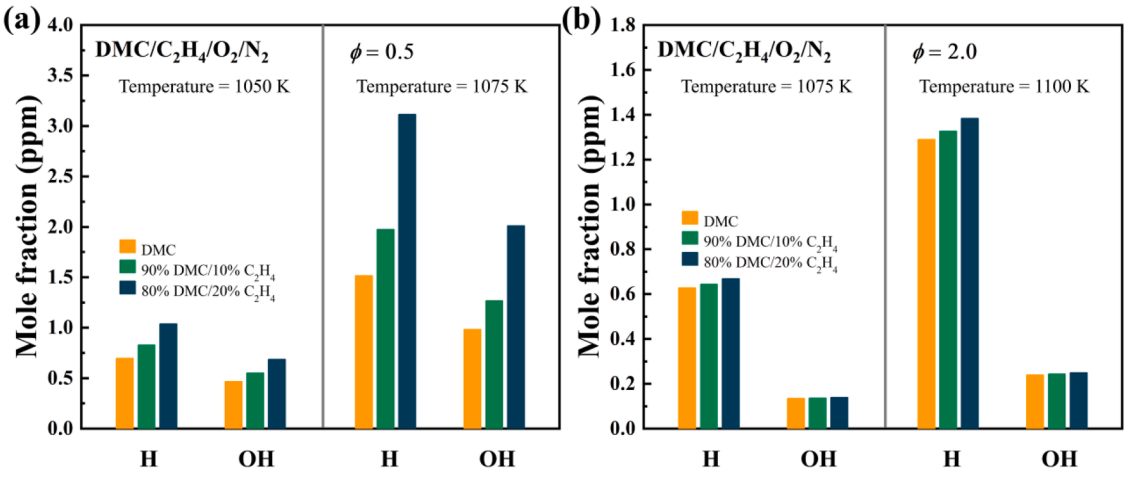

Fig. 10. Radical pool analysis of DMC blended with C_2H_4 using updated Alzueta's model. (a) 1050 K and 1075 K, $\phi = 0.5$, with 0 %, 10 %, and 20 % C_2H_4 blending; (b) 1075 K and 1100 K, $\phi = 2.0$, with 0 %, 10 %, and 20 % C_2H_4 blending.

oxidation of C_2H_4. Under fuel-rich condition, C_2H_4 blending leads to a non-monotonic evolution of the C_2H_4 mole fraction, characterized by a slight rise, followed by eventual depletion. This behavior primarily stems from the competition between the radical-driven C_2H_4 consumption and its regeneration driven by the DMC oxidation. The updated Alzueta's model, reasonably predict the experimental trends for the mole fraction of major species, but tend to overestimate the consumption of DMC above 1075 K and the mole fraction of minor species, such as DME and CH_4.

The mutual reaction mechanism between DMC and C_2H_4 oxidation elucidated in this study provides novel insights into the kinetic mechanisms governing thermal runaway (TR) and fire propagation in lithium-ion batteries (LiBs). The enhanced radical pool (O, OH) from C_2H_4 oxidation promotes DMC decomposition into flammable intermediates. C_2H_4 acts as both a co-fuel and a radical accelerator, sustaining combustion and amplifying the reaction rates of DMC and other volatile species. The non-monotonic behavior of C_2H_4 under fuel-rich conditions suggests a feedback loop where C_2H_4 regeneration sustains combustion, potentially leading to rapid fire propagation across battery cells in a pack. These mechanistic insights can inform the design of safer LiB systems.

CRediT authorship contribution statement

Bowen Liu: Writing – review & editing, Writing – original draft, Methodology, Investigation, Data curation. **Yuntian Guo:** Writing – review & editing, Methodology, Investigation. **Rui Bo:** Methodology, Investigation, Data curation. **Shuyan Guo:** Writing – review & editing, Data curation. **Hao Zhao:** Writing – review & editing, Supervision, Project administration, Methodology.

Declaration of competing interest

The authors declare that they have no known competing financial interests or personal relationships that could have appeared to influence the work reported in this paper.

Acknowledgments

This work was supported by the National Natural Science Foundation of China (Nos. 22361132538, 22350710788) and the National Key R&D Program of China grant (2022YFB2502100).

Supplementary materials

Supplementary material associated with this article can be found, in the online version, at doi:10.1016/j.combustflame.2025.114556.

References

[1] Y.-S. Duh, Y. Sun, X. Lin, J. Zheng, M. Wang, Y. Wang, X. Lin, X. Jiang, Z. Zheng, S. Zheng, G. Yu, Characterization on thermal runaway of commercial 18650 lithium-ion batteries used in electric vehicles: a review, J. Energy Storage 41 (2021) 102888.
[2] L. Lu, X. Han, J. Li, J. Hua, M. Ouyang, A review on the key issues for lithium-ion battery management in electric vehicles, J. Power Sources 226 (2013) 272–288.
[3] X. Feng, M. Ouyang, X. Liu, L. Lu, Y. Xia, X. He, Thermal runaway mechanism of lithium ion battery for electric vehicles: a review, Energy Storage Mater. 10 (2018) 246–267.
[4] Y. Fernandes, A. Bry, S. de Persis, Identification and quantification of gases emitted during abuse tests by overcharge of a commercial Li-ion battery, J. Power Sources 389 (2018) 106–119.
[5] N.E. Galushkin, N.N. Yazvinskaya, D.N. Galushkin, Mechanism of thermal runaway in lithium-ion cells, J. Electrochem. Soc. 165 (2018) 1303–1308.
[6] B. Nie, Y. Dong, L. Chang, The evolution of thermal runaway parameters of lithium-ion batteries under different abuse conditions: a review, J. Energy Storage 96 (2024) 112624.
[7] H. Wang, H. Xu, Z. Zhang, Q. Wang, C. Jin, C. Wu, C. Xu, J. Hao, L. Sun, Z. Du, Y. Li, J. Sun, X. Feng, Fire and explosion characteristics of vent gas from lithium-ion batteries after thermal runaway: a comparative study, Etransportation 13 (2022) 100190.
[8] G. Wei, R. Huang, G. Zhang, B. Jiang, J. Zhu, Y. Guo, G. Han, X. Wei, H. Dai, A comprehensive insight into the thermal runaway issues in the view of lithium-ion battery intrinsic safety performance and venting gas explosion hazards, Appl. Energy 349 (2023) 121651.
[9] D. He, J. Wang, Y. Peng, B. Li, C. Feng, L. Shen, S. Ma, Research advances on thermal runaway mechanism of lithium-ion batteries and safety improvement, Sustain. Mater. Technol 41 (2024) e01017.
[10] Q. Wang, P. Ping, X. Zhao, G. Chu, J. Sun, C. Chen, Thermal runaway caused fire and explosion of lithium ion battery, J. Power Sources 208 (2012) 210–224.
[11] D. Hu, S. Huang, Z. Wen, X. Gu, J. Lu, A review on thermal runaway warning technology for lithium-ion batteries, Renew. Sustain. Energy Rev. 206 (2024) 114882.
[12] Y. Li, N. Zhang, L. Jiang, Z. Wei, Y. Zhang, Y. Yu, L. Song, L. Wang, Q. Duan, J. Sun, Q. Wang, Assessment of the complete chain evolution process of LIBs from micro internal short circuit failure to thermal runaway under mechanical abuse conditions, Process. Saf. Environ. Prot. 185 (2024) 296–306.
[13] S. Wilke, B. Schweitzer, S. Khateeb, S. Al-Hallaj, Preventing thermal runaway propagation in lithium ion battery packs using a phase change composite material: an experimental study, J. Power Sources 340 (2017) 51–59.
[14] Y. Zhang, H. Wang, W. Li, C. Li, Quantitative identification of emissions from abused prismatic Ni-rich lithium-ion batteries, Etransportation 2 (2019) 100031.
[15] D. Ren, X. Feng, L. Lu, M. Ouyang, S. Zheng, J. Li, X. He, An electrochemical-thermal coupled overcharge-to-thermal-runaway model for lithium ion battery, J. Power Sources 364 (2017) 328–340.
[16] S. Koch, A. Fill, K.P. Birke, Comprehensive gas analysis on large scale automotive lithium-ion cells in thermal runaway, J. Power Sources 398 (2018) 106–112.
[17] J. Zhang, A. Zhong, Z. Huang, D. Han, Experimental and kinetic study on the stabilities and gas generation of typical electrolyte solvent components under oxygen-lean oxidation and pyrolysis conditions, Sci. China Technol. Sci. 65 (2022) 2883–2894.
[18] S. Jo, S. Seo, S.K. Kang, I. Na, S. Kunze, M. Song, S. Hwang, S.P. Woo, S. Kim, W. B. Kim, J. Lim, Thermal runaway mechanism in Ni-rich cathode full cells of lithium-ion batteries: the role of multidirectional crosstalk, Adv. Mater. 36 (2024) 2402024.
[19] K. Alexandrino, J. Salinas, Á. Millera, R. Bilbao, M.U. Alzueta, Sooting propensity of dimethyl carbonate, soot reactivity and characterization, Fuel 183 (2016) 64–72.
[20] M.U. Alzueta, P. Salinas, Á. Millera, R. Bilbao, M. Abián, A study of dimethyl carbonate conversion and its impact to minimize soot and NO emissions, Proc. Combust. Inst. 36 (2017) 3985–3993.
[21] W. Sun, B. Yang, N. Hansen, C.K. Westbrook, F. Zhang, G. Wang, K. Moshammer, C. K. Law, An experimental and kinetic modeling study on dimethyl carbonate (DMC) pyrolysis and combustion, Combust. Flame 164 (2016) 224–238.
[22] S. Suzuki, A. Matsugi, Experimental and modeling study of fuel-rich oxidation of gasoline surrogate components/dimethyl carbonate blends in an atmospheric flow reactor, Combust. Flame 261 (2024) 113332.
[23] H. Nakamura, H.J. Curran, A. Polo Córdoba, W.J. Pitz, P. Dagaut, C. Togbé, S. M. Sarathy, M. Mehl, J.R. Agudelo, F. Bustamante, An experimental and modeling study of diethyl carbonate oxidation, Combust. Flame 162 (2015) 1395–1405.
[24] H. Zhao, S. Liu, C. Yan, C. Huang, Y. Qi, F. Zhang, Y. Ju, Studies of ozone-sensitized low- and high-temperature oxidations of diethyl carbonate, J. Phys. Chem. A 125 (2021) 1760–1765.
[25] K. Kanayama, S. Takahashi, S. Morikura, H. Nakamura, T. Tezuka, K. Maruta, Study on oxidation and pyrolysis of carbonate esters using a micro flow reactor with a controlled temperature profile. Part I: reactivities of dimethyl carbonate, ethyl methyl carbonate and diethyl carbonate, Combust. Flame 237 (2022) 111810.
[26] K. Alexandrino, Á. Millera, R. Bilbao, M.U. Alzueta, Experimental and simulation study of the high pressure oxidation of dimethyl carbonate, Fuel 309 (2022) 122154.
[27] R. Shahla, C. Togbé, S. Thion, R. Timothée, M. Lailliau, F. Halter, C. Chauveau, G. Dayma, P. Dagaut, Burning velocities and jet-stirred reactor oxidation of diethyl carbonate, Proc. Combust. Inst. 36 (2017) 553–560.
[28] M. Henriksen, K. Vaagseather, A.V. Gaathaug, J. Lundberg, S. Forseth, D. Bjerketvedt, Laminar burning velocity of the dimethyl carbonate–air mixture formed by the Li-ion electrolyte solvent, Combust. Explos. Shock Waves 56 (2020) 383–393.
[29] T. Atherley, S. de Persis, N. Chaumeix, Y. Fernandes, A. Bry, A. Comandini, O. Mathieu, S. Alturaifi, C.R. Mulvihill, E.L. Petersen, Laminar flame speed and shock-tube multi-species laser absorption measurements of dimethyl carbonate oxidation and pyrolysis near 1 atm, Proc. Combust. Inst. 38 (2021) 977–985.
[30] X. Li, W. Xu, Y. Li, Y. Jiang, Investigation of laminar burning velocities and cellular instability for dimethyl carbonate at elevated pressures, Energy Fuels 35 (2021) 6210–6218.
[31] M.E. Bardin, E.V. Ivanov, E.J.K. Nilsson, V.A. Vinokurov, A.A. Konnov, Laminar burning velocities of dimethyl carbonate with air, Energy Fuels 27 (2013) 5513–5517.
[32] E. Hu, Y. Chen, Z. Zhang, L. Pan, Q. Li, Y. Cheng, Z. Huang, Experimental and kinetic study on ignition delay times of dimethyl carbonate at high temperature, Fuel 140 (2015) 626–632.
[33] K. Alexandrino, M.U. Alzueta, H.J. Curran, An experimental and modeling study of the ignition of dimethyl carbonate in shock tubes and rapid compression machine, Combust. Flame 188 (2018) 212–226.
[34] R. Yu, J. Liu, Y. Wu, C. Tang, W. Liang, H. Wang, M. Ouyang, Experimental and modeling study of the ignition kinetics of dimethyl carbonate, Combust. Flame 246 (2022) 112465.
[35] P. Dagaut, M. Cathonnet, J.P. Rouan, R. Foulatier, A. Quilgars, J.C. Boettner, F. Gaillard, H. James, A jet-stirred reactor for kinetic studies of homogeneous gas-phase reactions at pressures up to ten atmospheres (≈ 1 MPa), J. Phys. E: Sci. Instrum. 19 (1986) 207.
[36] Chemkin-Pro, Release 15112, Reaction Design, 422, Inc, San Diego CA, 2011, p. 396.
[37] W.K. Metcalfe, S.M. Burke, S.S. Ahmed, H.J. Curran, A hierarchical and comparative kinetic modeling study of C1- C2 hydrocarbon and oxygenated fuels, Int. J. Chem. Kinet. 45 (2013) 638–675.
[38] P.A. Glaude, W.J. Pitz, M.J. Thomson, Chemical kinetic modeling of dimethyl carbonate in an opposed-flow diffusion flame, Proc. Combust. Inst. 30 (2005) 1111–1118.